ARMY RESEARCH LABORATORY

High-Temperature Transitions in Metallopolymers Crosslinked With 2,6-bis(1'-methylbenzimidazolyl)pyridine Metal-Ligand Complex

by Aaron C. Jackson, Robert H. Lambeth, Victor Rodriguez-Santiago, Brady G. Butler, and Frederick L. Beyer

ARL-TR-6706 **October 2013**

NOTICES

Disclaimers

The findings in this report are not to be construed as an official Department of the Army position unless so designated by other authorized documents.

Citation of manufacturer's or trade names does not constitute an official endorsement or approval of the use thereof.

Destroy this report when it is no longer needed. Do not return it to the originator.

Army Research Laboratory
Aberdeen Proving Ground, MD 21005-5066

ARL-TR-6706 **October 2013**

High-Temperature Transitions in Metallopolymers Crosslinked With 2,6-bis(1'-methylbenzimidazolyl)pyridine Metal-Ligand Complex

Aaron C. Jackson, Robert H. Lambeth, Victor Rodriguez-Santiago, Brady G. Butler, and Frederick L. Beyer
Weapons and Materials Research Directorate, ARL

REPORT DOCUMENTATION PAGE	Form Approved OMB No. 0704-0188

1. REPORT DATE *(DD-MM-YYYY)*	2. REPORT TYPE	3. DATES COVERED (From - To)
October 2013	Final	September 2012–August 2013

4. TITLE AND SUBTITLE
High-Temperature Transitions in Metallopolymers Crosslinked With 2,6-bis(1'-methylbenzimidazolyl)pyridine Metal-Ligand Complex

5a. CONTRACT NUMBER

5b. GRANT NUMBER

5c. PROGRAM ELEMENT NUMBER

6. AUTHOR(S)
Aaron C. Jackson, Robert H. Lambeth, Victor Rodriguez-Santiago, Brady G. Butler, and Frederick L. Beyer

5d. PROJECT NUMBER

5e. TASK NUMBER

5f. WORK UNIT NUMBER

7. PERFORMING ORGANIZATION NAME(S) AND ADDRESS(ES)
U.S. Army Research Laboratory
ATTN: RDRL-WMM-G
Aberdeen Proving Ground, MD 21005-5066

8. PERFORMING ORGANIZATION REPORT NUMBER
ARL-TR-6706

9. SPONSORING/MONITORING AGENCY NAME(S) AND ADDRESS(ES)

10. SPONSOR/MONITOR'S ACRONYM(S)

11. SPONSOR/MONITOR'S REPORT NUMBER(S)

12. DISTRIBUTION/AVAILABILITY STATEMENT
Approved for public release; distribution is unlimited.

13. SUPPLEMENTARY NOTES

14. ABSTRACT
Metallopolymers have reversible bonding properties and strong phase separation behavior that make them useful for a variety of applications. However, relaxation processes within the polymer, specifically relaxation processes within the metal-ligand (ML) rich phase, are not fully understood. This report proposes that scission of the ML bond and softening of the ML-rich phase within the polymer are the primary relaxation processes occurring above room temperature. Dynamic mechanical analysis (DMA) tests show that both play a role in the degradation of the mechanical properties above 100 °C. In polymers containing cobalt and iron, the two relaxation processes were separate while these relaxation processes were interdependent in polymers containing copper and zinc. Under static conditions, no relaxation processes were evident as measured by ultraviolet/visible (UV/Vis) light spectroscopy, small-angle x-ray scattering (SAXS), and x-ray diffraction (XRD). These results highlight the importance of the ligand chemistry and counter ion, two components of metallopolymers that may have a large impact on the softening point of the ML-rich phase. They also highlight a need to study changes in the morphology and spectral response of metallopolymer under mechanical stress.

15. SUBJECT TERMS
metallopolymer, phase separation, mechanical properties

16. SECURITY CLASSIFICATION OF:			17. LIMITATION OF ABSTRACT	18. NUMBER OF PAGES	19a. NAME OF RESPONSIBLE PERSON
a. REPORT	b. ABSTRACT	c. THIS PAGE			Frederick L. Beyer
Unclassified	Unclassified	Unclassified	UU	26	19b. TELEPHONE NUMBER (*Include area code*) 410-306-0893

Standard Form 298 (Rev. 8/98)
Prescribed by ANSI Std. Z39.18

Contents

List of Figures

List of Tables

INTENTIONALLY LEFT BLANK.

1. Introduction

A supramolecular polymer is a class of polymers held together by noncovalent, reversible bonds (*1–4*). Types of supramolecular bonds include π-π stacking, (*5–8*) hydrogen bonding, (*9–13*) and metal-ligand (ML) bonds (*14–21*). These bonds break as a result of light exposure, high temperature, the presence of competing ions, or mechanical stress. As the bonds break, the molecular weight of the polymer changes drastically, allowing reorganization of the polymer. The supramolecular polymers developed and described in this report are metallopolymers whose reversible bonds are derived from ML bonds.

One important difference between metallopolymers and other supramolecular polymers is that the strength and kinetics of bond formation in metallopolymers can be adjusted by changing the metal ion and not the underlying chemistry of the polymer. Tridentate, pyridine-based ligands such as terpyridine (TPY) or 2,6-bis(1'-methylbenzimidazolyl)pyridine (MeBIP) create particularly strong ML bonds (*14–18*). Of the library of metal-ions studied, copper(II), cobalt(II), zinc(II), and iron(II) have a range of disparate bond strengths (table 1) and are studied for their effects on polymer film properties here. The bonding of Cu(II) to TPY or MeBIP is particularly weak (*22–24*). Dobrawa and Wurthner (25) show that zinc(II) binds weakly to TPY (*25*), but others demonstrate robust metallopolymer formation with MeBIP ligands (*14–16*). Cobalt(II) and iron(II) have particularly strong binding behavior with TPY and MeBIP (*22–26*).

Table 1. Binding constant and ΔH^0_{rxn} for relevant metal ions complexed with TPY.

Metal ion/Ligand	**Binding Constant (K_1) in Water (M^{-1}) (*23*)**	**ΔH^0_{rxn} (kJ/mol) (*24*)** ***Rxn: $M(tpy)^{2+} + tpy \leftrightarrow M(tpy)_2^{2+}$*** ***Solvent: Acetonitrile***
Fe^{2+}/TPY	1.3×10^7	–79.9
Co^{2+}/TPY	2.5×10^8	–61.5
Zn^{2+}/TPY	1.0×10^6	–60.7
Cu^{2+}/TPY	—	–54.4

Another defining feature of metallopolymers is consistent and strong phase separation. Phase separation is more frequently observed in metallopolymers than in other supramolecular polymers due to the high aromaticity and ionic nature of the ML complex. In linear metallopolymers, polymers where the ligand is attached to the terminal positions of the polymer chain, phase separation leads to a lamellar morphology within the polymer (*14*, *17*, *18*). Within the lamellar region, the ML complexes order on the molecular level as observed by wide-angle x-ray scattering (WAXS) (*14*). When poly(tetrahydrofuran) (PTHF) is the linking polymer, the phase separation results in a polymer with a modest, approximately 10 MPa, storage modulus at

temperatures above the expected melting temperature of PTHF (*14*, *15*). In poly(butyl acrylate) cross-linked with ML bonds, phase separation also occurs and results in a polymer that is ten times stiffer than the stiffness predicted by the theory of rubber elasticity (*27*).

The work described in this report proposes bond scission of the ML complex and softening of the ML-rich phase as two relaxation processes that affect the melting point of metallopoylmers. Bond scission is expected to occur in these polymers due to the relatively low-bond energies associated with ML complexes. Several reports document scission of the ML complex at high temperatures, under radiation, or under mechanical load (*14*, *15*, *17*, *18*, *26*). While a softening transition within the ML-rich phase has not been discussed in the literature, several researchers noted that the ML-rich phase acts as physical cross-links. Beck, et al. and Kumpfer, et al. attribute a rubbery plateau in end-functionalized poly(tetrahydrofuran) to phase separation (*14*) and physical cross-links (*15*). In our previous research (*27*), a particularly high-rubbery plateau modulus also suggested that the ML-rich phase of poly(butyl acrylate) cross-linked with ML bonds also acts as physical cross-links. Based on x-ray diffraction (XRD) from those works, the ML-rich phase is amorphous and, as a result, the transition associated with it is expected to be a glass transition with an associated T_g.

Determination of the relaxation processes in the ML-rich phase is important for improving mechanical properties and developing appropriate manufacturing conditions for metallopolymers. On the one hand, the choice of metal ion is important and leads to gels and polymer films with different properties (*14*, *15*, *17*). On the other hand, adjusting the T_g of the ML-rich phase requires new ligands or different counter ions, but these are aspects of the metallopolymer system that have not been studied extensively. To understand the relaxation processes better, this work investigates the high-temperature mechanical, optical, and morphological properties of poly(butyl acrylate) cross-linked with ML bonds. Previous work described the synthesis of this polymer and its properties up to 100 °C (*27*). The polymer system is particularly useful for this work since it isolates the relaxation processes of the ML-rich phase.

2. Materials and Methods

2.1 Materials

All solvents and reagents were purchased from commercial sources and used as received unless otherwise mentioned. Azobisisobutyronitrile (AIBN) was twice recrystallized from MeOH. Butyl acrylate was passed over basic alumina and stored in a freezer. Compound **1 (**Scheme 1) was prepared according to procedures described by Rowan and Beck (*28*). Compounds **2**, **3**, and **4** were prepared as described by Jackson, et al. (*27*).

2.2 Film Formation

Three types of films were manufactured. Cast films (Cast 4-M) were manufactured by dissolving the polymer and metal ion (0.2 mmol per gram polymer) in a solution of acetonitrile and chloroform (1 : 1 solvent ratio, <5% polymer concentration). Either $Cu(ClO_4)_2$ (**4**-Cu), $Co(ClO_4)_2$ (**4**-Co), $Zn(ClO_4)_2$ (**4**-Zn), or $Fe(ClO_4)_2$ (**4**-Fe) were used as the metal ion source. The solutions were poured into Teflon dishes, covered, and kept at room temperature. After the solvent evaporated, the films were annealed at 80 °C to remove excess solvent (Cast **4**-M). A quicker casting process was used to initiate the pressed film process (Pressed **4**-M). Solutions were left uncovered to evaporate and, once the solvent was removed, the polymer was hot pressed. To do this, the sample was placed between two metal plates with kapton spacers. When under pressure, 100 psi of pressure was applied to the layup. The hot press cycle followed the procedure: (1) 30 min at 200 °C, no pressure, (2) 10 min at 200 °C, pressure, (3) cool from 200 to 60 °C over 4 h under pressure. All film formation steps were done in air.

2.3 Analytical

Dynamic mechanical analysis (DMA) data were taken using a DMA Q800 from TA Instruments with tensile grips. Temperature sweeps were taken at 1 hertz (Hz). Ultraviolet/visible (UV/Vis) spectra of samples were taken using a Perkin Elmer 950. Samples were cast onto glass cover slides in a procedure similar to the casting method described in section 2.2. During high-temperature UV/Vis experiments, the sample was sandwiched between two metal plates across a slit in each plate for UV/Vis collection. Heating pads attached to the metal plates provided heat to the sample. The difference between the recorded temperature and the actual sample temperature was as high as 10 °C up to 140 °C. Differential scattering calorimetry (DSC) was performed on a TA Instruments Q1000. All samples were run from –80 to 200 °C at 5 °C/min. ^{1}H nuclear magnetic resonance (NMR) spectroscopy was performed on a Bruker 600 MHz instrument. Samples were run in deuterated chloroform and chemical shifts are reported in parts per million (ppm) as referenced from the residual solvent peak. Coupling constants are reported in Hertz.

Small-angle x-ray scattering (SAXS) data were collected using a Molecular Metrology area detector. Ni-filtered CuKα x-ray radiation (λ = 1.542 Å) was produced using a Rigaku Ultrax18 x-ray generator operated at 45 kV and 100 mA. Data collected at camera lengths of 150 cm and 50 cm were merged into continuous data sets spanning scattering vector magnitude, q, ranging from 0.007 $Å^{-1}$ to 0.45 $Å^{-1}$. The instrument was calibrated using silver behenate for distance and beam center, and glassy carbon for intensity. Data were corrected for sample absorption and background noise before scaling to absolute intensity (cm^{-1}). The two-dimensional data sets were azimuthally averaged to give intensity as a function of q, where $q = 4\pi \cdot \sin(\theta)/\lambda$ and 2θ is the scattering angle. All data processing and analysis were performed using IGOR Pro 6 (WaveMetrics, Inc.) and tool suites available from Argonne National Laboratory (*29*). High-temperature SAXS was performed using a Molecular Metrology temperature control cell

with water cooling. The sample was sandwiched between two kapton films within the control cell. Data correction via a secondary sample was not possible and all measurements are absolute and include a peak from the caption film at 0.3 $Å^{-1}$.

Near-surface compositional depth profiling of the as-deposited coatings was performed using the Kratos Axis Ultra x-ray photoelectron spectroscopy system, equipped with a hemispherical analyzer. A 100 W monochromatic Al Kα (1486.7 eV) beam irradiated a 1 mm × 0.5 mm sampling area with a take-off angle of 90°. The base pressure in the x-ray photoelectron spectroscopy (XPS) chamber was held between 10^{-9} and 10^{-10} Torr. Elemental high-resolution scans for Fe_{2p} and Co_{2p} core levels were taken in the constant analyzer energy mode with 80 eV pass energy. The sp^3 C_{1s} peak was used as reference for binding energy calibration.

X-ray diffraction measurements were performed on a Panalytical X'Pert Pro Materials Research Diffractometer system using CuKα radiation (λ = 0.15406 nm) and a step size of 0.05° 2θ. Elevated temperature measurements were conducted using an Anton Paar HTK 2000N nonambient stage. Diffraction measurements were taken in 20° increments from room temperature to 200 °C with a 10-min hold-time before each measurement to minimize transient heating effects. There was no distinguishable difference between room temperature diffraction patterns before and after heating, indicating that the peak shifts are fully reversible. The d-spacing associated with the peaks for each sample and temperature was calculated by fitting the local curve to a quadratic function and calculating the d-spacing from the maximum in the quadratic function.

3. Results and Discussion

Reversible addition fragmentation chain transfer (RAFT) polymerization of monomer **3** and n-butyl acrylate resulted in a low T_g polymer with MeBIP side groups (Scheme 1) (see figure 1). NMR confirmed the incorporation of MeBIP groups to the polymer backbone (figure 2a) and showed that excess MeBIP monomer was removed from the sample. Based on UV/Vis titrations (figure 2b), polymer **4** contained 0.4-mmol MeBIP per gram of polymer. This was derived from the quantity of $Zn(ClO_4)_2$ required for the two peaks characteristic of the free MeBIP and Zn-MeBIP complex to reach a saturation point. This technique is common in literature and works as a result of the high-binding constant between Zn(II) and MeBIP (*24*, *27*).

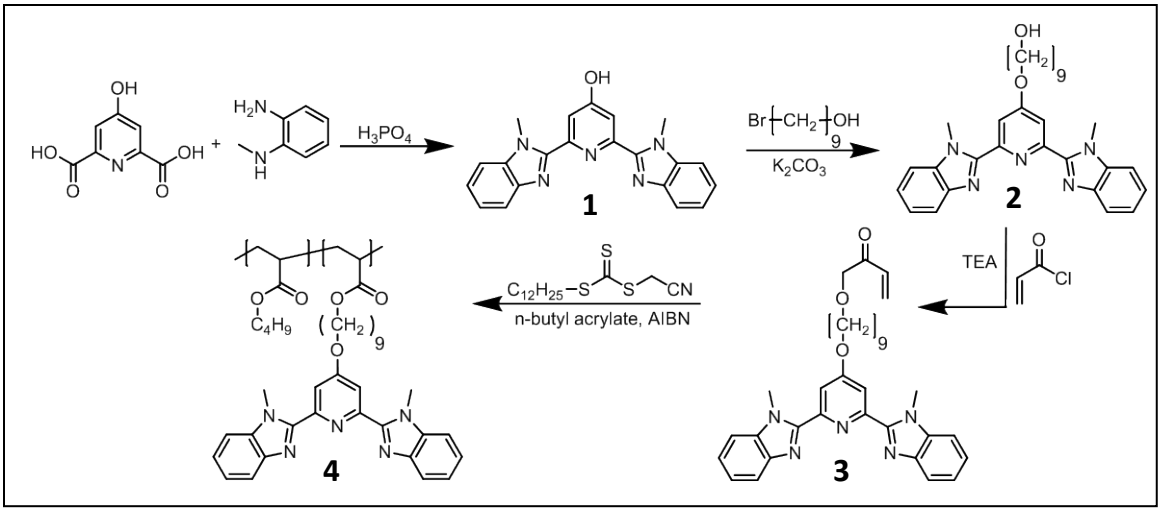

Figure 1. Scheme 1: Synthesis scheme for polymer **4**.*

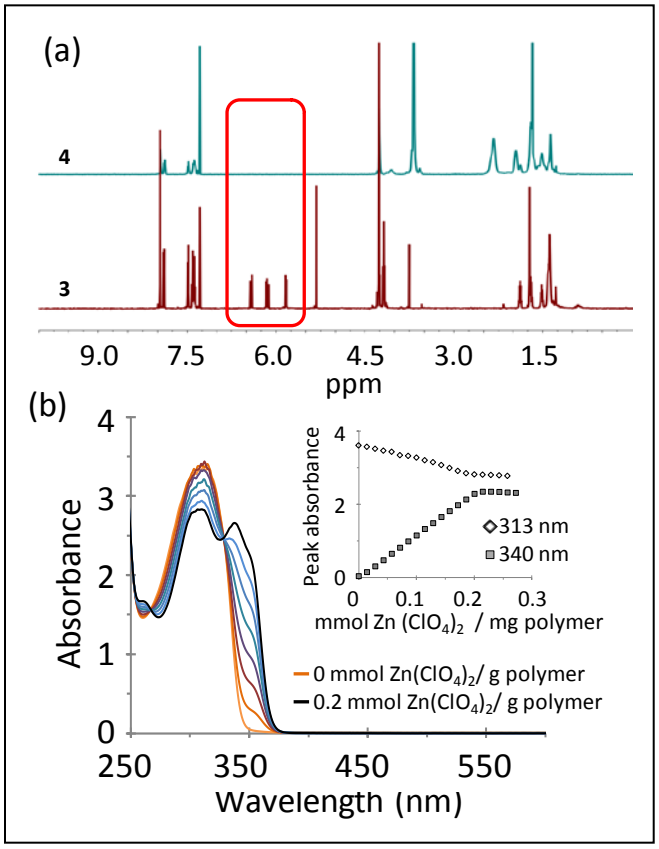

Figure 2. NMR (a) comparing polymer **4** and monomer 3, and UV/Vis titration (b) of polymer **4**.*

*Figures 1 and 2 reproduced with permission of copyright owner (see reference 27).

For each polymer tested, DMA of cast and pressed polymers showed that the degradation of the mechanical properties are dependent on the metal ion and this is consistent with the expected ML bonding strength (figure 3). Based on the sharp increase in tan(δ), or decrease in the storage modulus at high temperatures, it was evident that the metal ion choice does influence the melting point of the metallopolymers. The melting point trend was independent of the processing conditions, despite differences in the morphology between cast and pressed films discussed previously (*27*). The trend matched the strength of the ML bond such that $T_{m,\mathbf{4}\text{-Cu}} < T_{m,\mathbf{4}\text{-Zn}} < T_{m,\mathbf{4}\text{-Co}}$. However, these melting temperatures are not well defined by DMA.

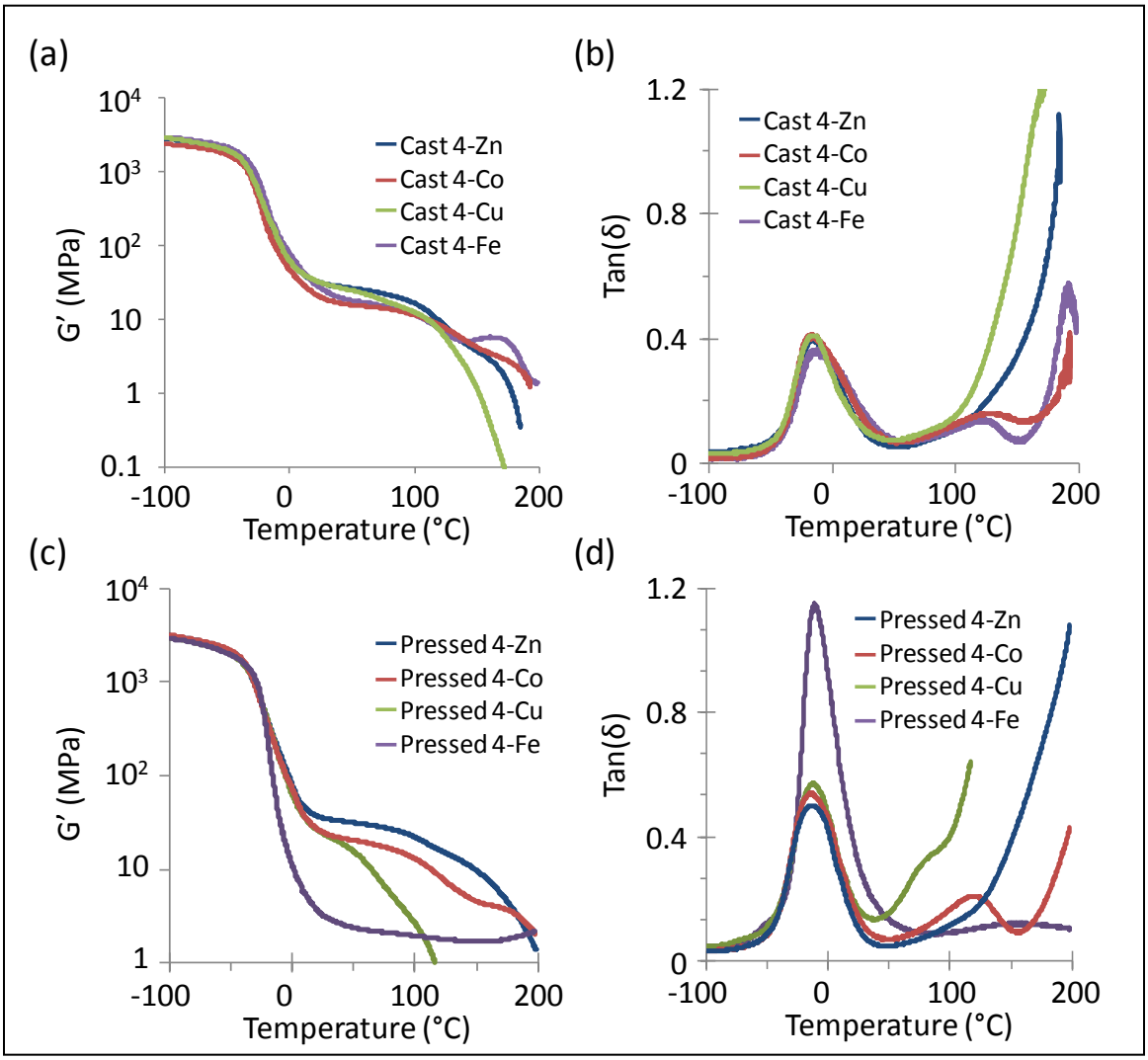

Figure 3. Storage modulus and tan(δ) of cast films (a and b, respectively) and pressed films (c and d respectively).

The melting temperature of cast **4**-Fe is not clear from the DMA data because the slope of the storage modulus is positive at high temperatures for both cast and pressed **4**-Fe. In addition, the behavior of pressed **4**-Fe differed markedly from cast **4**-Fe. XPS of films of pressed **4**-Fe

(figure 4) suggested that oxidation occurred during the manufacture of the films since Fe(III) was present in addition to Fe(II). Based on peaks obtained from previous literature (*31*, *32*), the peak at 709.5 eV corresponds to Fe(II) while the peak at 712.5 eV corresponds to Fe(III). These peaks correspond to an atomic ratio of 1.18:1 Fe(II): Fe(III). Since Fe(III) binds poorly with TPY (*17*), it is expected to bind poorly with MeBIP. This is consistent with the particularly low-rubbery plateau modulus for pressed **4**-Fe and may play a role in the increasing storage modulus of **4**-Fe at high temperature.

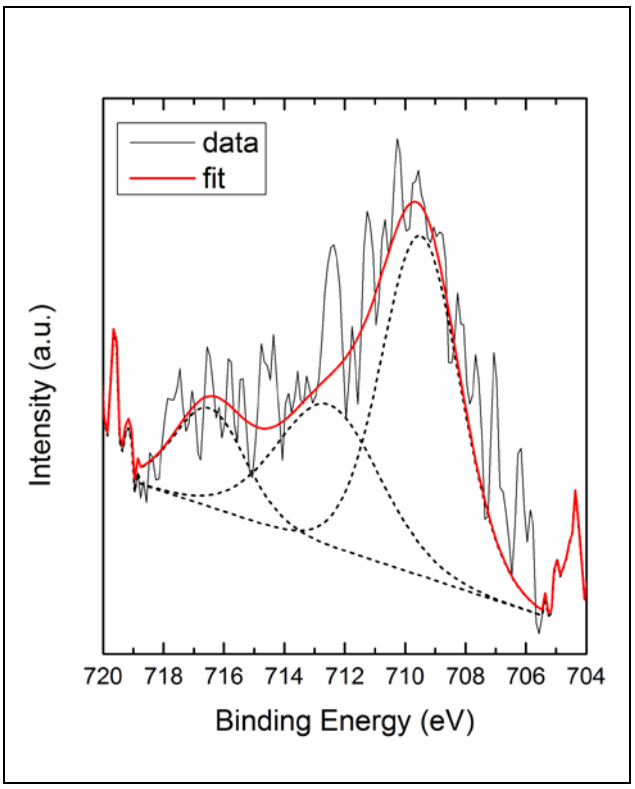

Figure 4. XPS of pressed **4**-Fe. Dotted lines correspond to contributions to the fit from each potential source.

Oxidation is also possible in **4**-Co where Co(II) is converted to Co(III). In metallopolymers based on TPY and **1**, oxidation of cobalt does not degrade the polymer's mechanical properties because the Co(III) complex is stronger than the Co(II) complex (*29*). For example, Mugemana, et al. oxidized Co(II) to form a kinetically inert complex for their block copolymer system (*30*). XPS of a powder of **1**-Co cast from a solution of chloroform and acetonitrile showed that Co(III) was present in addition to Co(II). Figure 5 shows two main structures for the Co_{2p} core level, which indicate the orbital-spin splitting for $Co_{2p3/2}$ (777 eV – 797 eV) and $Co_{2p1/2}$ (797 eV – 810 eV) electrons. The $Co_{2p3/2}$ peak was used for analysis. Based on previous

literature, the peak at 780.9 corresponds to Co(II) and the peak at 782.1 corresponds to Co(III) (*33*, *34*). The atomic ratio, based on integration of the peaks, was 0.4:1 Co(II):Co(III). This oxidation occurred prior to the pressing phase and points to the possibility that oxidation occurs early in the manufacturing process of metallopolymers.

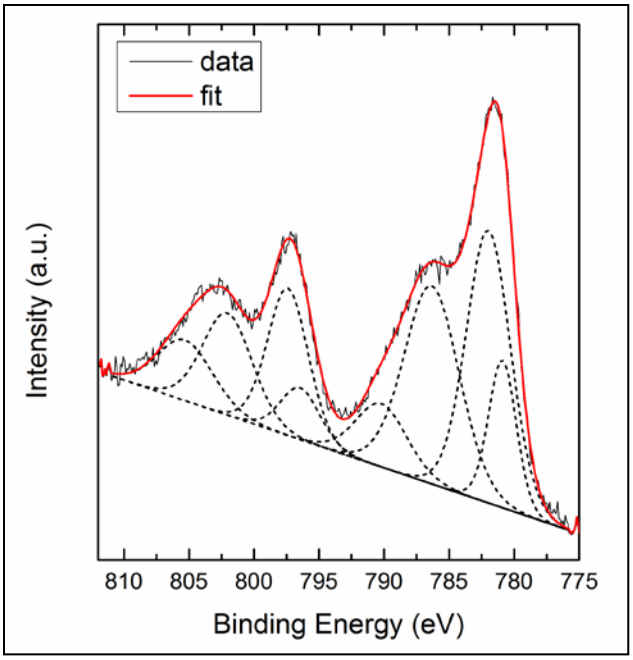

Figure 5. XPS of cast **1**-Co. Dotted lines correspond to contributions to the fit from each potential source.

Based on changes in curvature in tan(δ) and the storage modulus, the melting transition of these metallopolymers could not be ascribed to a single relaxation mechanism. This is most evident for **4**-Co and cast **4**-Fe. The peak in tan(δ) near 120 °C suggested that two independent relaxations occurred as the polymer's mechanical properties degraded. Changes in curvature of **4**-Cu and **4**-Zn suggested that similar relaxations also occurred in those polymers. Since there was not a peak in tan(δ), the relaxation mechanisms in **4**-Cu and **4**-Zn were likely interdependent.

Despite the observed transitions in the mechanical properties, similar transitions did not occur under static conditions. UV/Vis showed no changes in the ML bonding up to 140 °C (figure 6). SAXS showed no changes in the morphology up to 260 °C (figure 7). DSC of **4**-Cu and **4**-Co showed no readily apparent thermodynamic transitions although the low volume fraction of the ML-rich phase makes it difficult to differentiate potential transitions from artifacts (figure 8). Only linear changes in molecular spacing occurred upon heating the polymers to 200 °C (figure 9). Those changes occurred in the XRD peak at approximately 2θ=20°. According to Beck, et al., (*14*) this peak corresponds to amorphous structure in the ML-rich phase. As a result, these changes correspond to thermal expansion of the ML-rich phase. The lack of observed transitions in the static metallopolymer suggests that the changes in the metallopolymer system observed in

DMA are mechanically activated. It is possible that changes in UV/Vis, SAXS, DSC, or XRD may occur after longer time periods. However, annealing **4**-Zn at 200 °C for 48 h resulted in discolored samples and suggested that the polymer undergoes partial chemical degradation if exposed to high temperatures beyond those experienced during the pressing process.

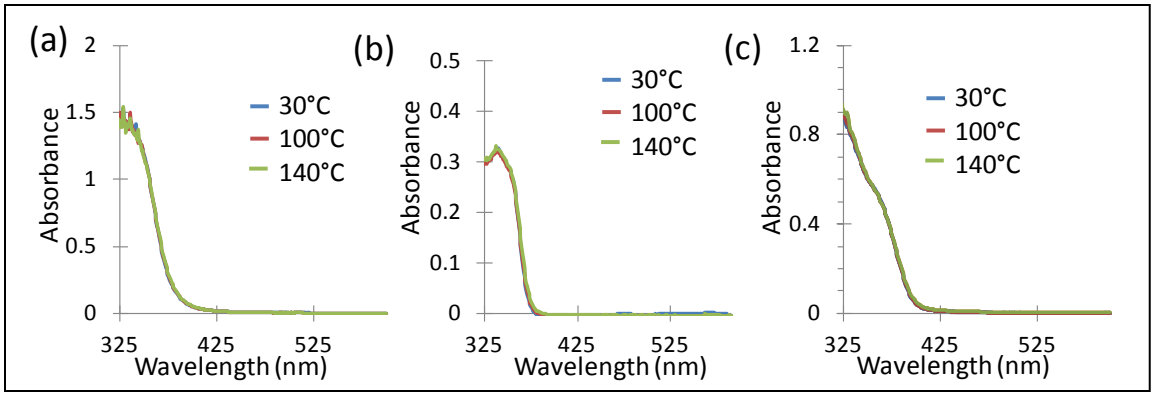

Figure 6. UV/Vis from room temperature to 140 °C for **4**-Co (a), **4**-Zn (b), and **4**-Cu (c). At 140 °C, the sample temperature differs from the reading temperature by up to 10 °C.

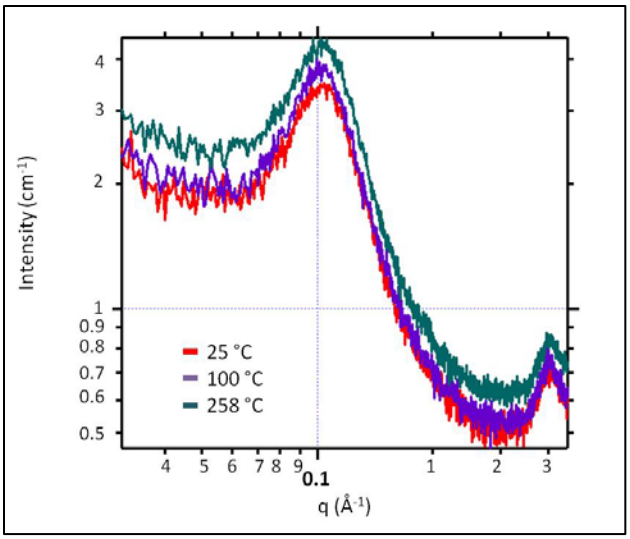

Figure 7. SAXS of **4**-Co from room temperature to 258 °C.

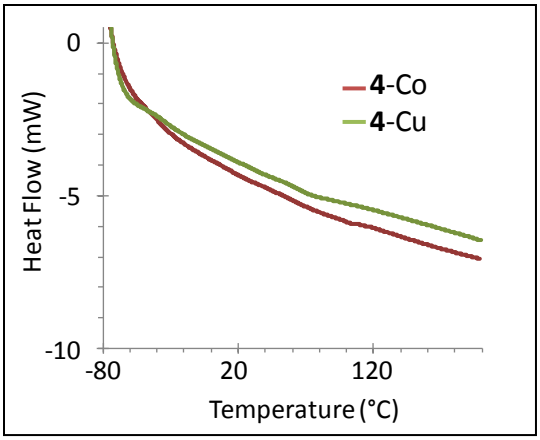

Figure 8. DSC of **4**-Cu and **4**-Co.

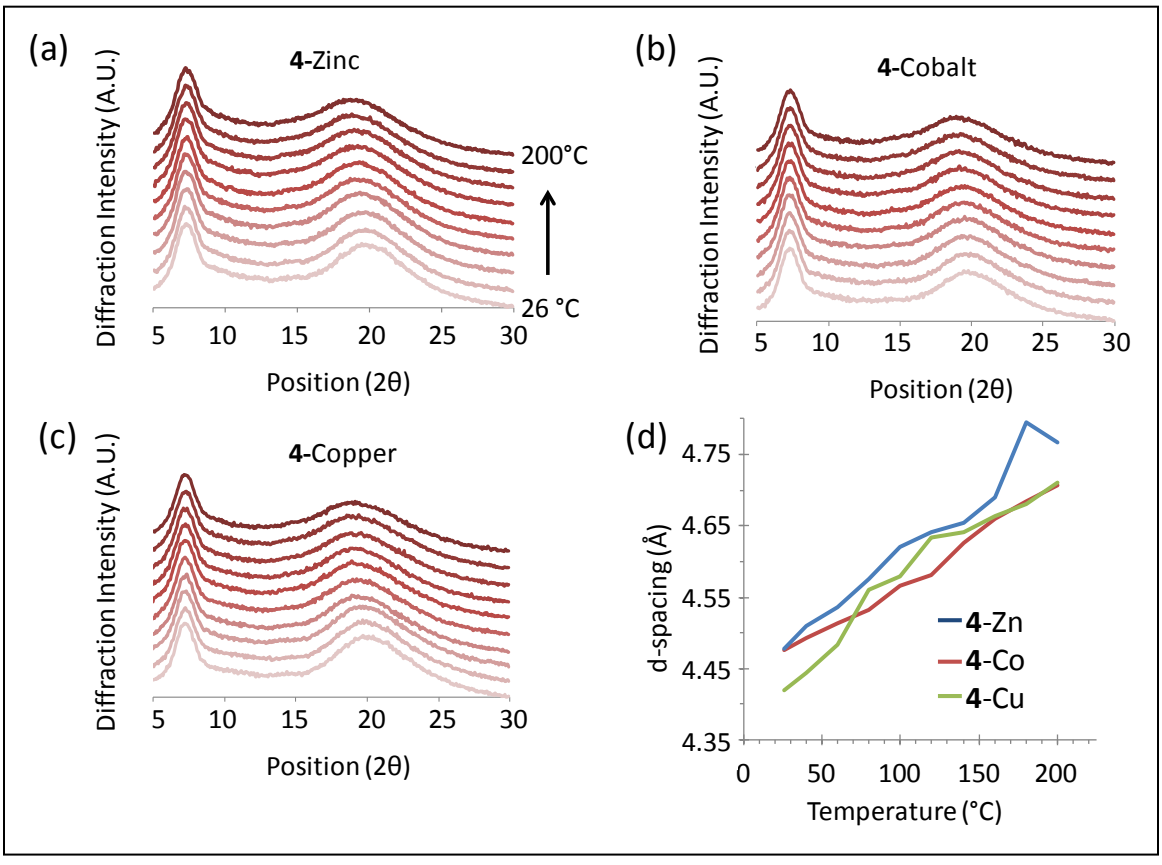

Figure 9. XRD of **4**-Co (a), **4**-Zn (b), and **4**-Cu (c) at room temperature (light red) up to 200 °C (dark red) in 20 °C increments. The d-spacing corresponding to the XRD peak at ca. 2θ = 20° is plotted as a function of temperature (d) for each polymer.

4. Conclusions

In conclusion, DMA data showed that multiple relaxation processes occur in the ML-rich phase of poly(butyl acrylate) cross-linked with ML bonds. However, these relaxation processes did not occur under static conditions as observed by UV/Vis, SAXS, DSC, and XRD. These results suggest several future avenues of study in metallopolymers. Oxidation in these polymers was evident from XPS and should be studied further to eliminate or take advantage of it. The effects of the counter ion and chemistry of the ligand should be studied further to understand how each affects the T_g of the ML-rich phase. For example, these components can be modified to eliminate phase separation to isolate the effects of the metal ion on the mechanical properties of metallopolymers. Finally, to better separate ML bond scission and softening in the ML-rich phase, future study of changes in spectral response and morphology should be studied under mechanical stress.

INTENTIONALLY LEFT BLANK.

5. References

1. Brunsveld, L.; Folmer, B. J. B.; Meijer, E. W.; Sijbesma, R. P. Supramolecular Polymers. *Chem. Rev.* **2001**, *101* (12), 4071–4097.
2. Fox, J. D.; Rowan, S. J. Supramolecular Polymerizations and Main-Chain Supramolecular Polymers. *Macromolecules* **2009**, *42* (18), 6823–6835.
3. de Greef, T. F. A.; Meijer, E. W. Materials Science: Supramolecular Polymers. *Nature* **2008**, *453* (7192), 171–173.
4. Rowan, S. J. Metallomesogens. *Angew Chem. Int. Ed.* **2005**, *44*, (31) 4830–4832.
5. Burattini, S.; Greenland, B. W.; Merino, D. H.; Weng, W.; Seppala, J.; Colquhoun, H. M.; Hayes, W.; Mackay, M. E.; Hamley, I. W.; Rowan, S. J. A Healable Supramolecular Polymer Blend Based on Aromatic π-π Stacking And Hydrogen Bonding Interactions. *J. Am. Chem. Soc.* **2010**, *132* (34), 12051–12058.
6. Burattini, S.; Greenland, B. W.; Hayes, W.; Mackay, M. E.; Rowan, S. J.; Colquhoun, H. M. A Supramolecular Polymer Based on Tweezer-Type π-π Stacking Interactions: Molecular Design for Healability And Enhanced Toughness. *Chem. Mater.* **2011**, *23* (1), 6–8.
7. Colquhoun, H. M.; Williams, D. J.; Zhu, Z. Versatile Supramolecular Receptors with Extreme Thermochemical and Oxidative Stability. *J. Am. Chem. Soc.* **2002**, *124* (45), 13346–13347.
8. Sivakova, S.; Bohnsack, D. A.; Mackay, M. E.; Suwanmala, P.; Rowan, S. J. Utilization of a Combination of Weak Hydrogen Bonding Interactions and Phase Segregation to Yield Highly Thermo-Sensitive Supramolecular Polymers. *J. Am. Chem. Soc.* **2005**, *127* (51), 18202–18211.
9. Cordier, P.; Tournilhac, F.; Soulie-Ziakovic, C.; Leibler, L. Self-Healing And Thermoreversible Rubber From Supramolecular Assembly. *Nature* **2008**, *451* (7181), 977–980.
10. Colquhoun, H. M. Self-Repairing Ploymers: Materials that Heal Themselves. *Nat. Chem.* **2012**, *4* (6), 435–436.
11. van Beek, D. J. M.; Spiering, A. J. H.; Peters, G. W. M.; te Nijenhuis, K.; Sijbesma, R. P. Unidirectional Dimerization and Stacking of Ureidopyrimidinone End Groups in Polycaprolactone Supramolecular Polymers. *Macromolecules* **2007**, *40* (23), 8464–8475.

12. Hirschberg, J.; Beijer, F. H.; van Aert, H. A.; Magusin, P.; Sijbesma, R. P.; Meijer, E. W. Supramolecular Polymers from Linear Telechelic Siloxanes with Quadruple-Hydrogen-Bonded Units. *Macromolecules* **1999**, *32* (8), 2696–2705.

13. Rowan, S. J.; Suwanmala, P.; Sivakova, S. Nucleobase-Induced Supramolecular Polymerization in The Solid State. *J. Polym. Sci., Part A: Polym. Chem.* **2003**, *41* (22), 3589–3596.

14. Beck, J. B.; Ineman, J. M.; Rowan, S. J. Metal/Ligand-Induced Formation of Metallo-Supramolecular Polymers. *Macromolecules* **2005**, *38* (12), 5060–5068.

15. Kumpfer, J. R.; Jin, J.; Rowan, S. J. Stimuli-Responsive Europium-Containing Metallo-Supramolecular Polymers. *J. Mater. Chem.* **2010**, *20* (1), 145–151.

16. Schmatloch, S.; Gonzalez, M. F.; Schubert, U. S. Metallo-Supramolecular Diethylene Glycol: Water-Soluble Reversible Polymers. *Macromol. Rapid Commun.* **2002**, *23* (16), 957–961.

17. Schmatloch, S.; van den Berg, A. M. J.; Alexeev, A. S.; Hofmeier, H.; Schubert, U. S. Soluble High-Molecular-Mass Poly(ethylene oxide)s via Self-Organization. *Macromolecules* **2003**, *36* (26), 9943–9949.

18. Burnworth, M.; Tang, L.; Kumpfer, J. R.; Duncan, A. J.; Beyer, F. L.; Fiore, G. L.; Rowan, S. J.; Weder, C. Optically Healable Supramolecular Polymers. *Nature* **2011**, *472* (7343), 334–337.

19. Burnworth, M.; Mendez, J. D.; Schroetert, M.; Rowan, S. J.; Weder, C. Decoupling Optical Properties in Metallo-Supramolecular Poly(*p*-phenylene ethynylene)s. *Macromolecules* **2008**, *41* (6), 2157–2163.

20. Yount, W. C.; Juwarker, H.; Craig, S. L. Orthogonal Control of Dissociation Dynamics Relative to Thermodynamics in a Main-Chain Reversible Polymer. *J. Am. Chem. Soc.* **2003**, *125* (50), 15302–15303.

21. Xu, D.; Liu, C.; Craig, S. L. Divergent Shear Thinning and Shear Thickening Behavior of Supramolecular Polymer Networks in Semidilute Entangled Polymer Solutions. *Macromolecules* **2011**, *44* (7), 2343–2353.

22. Hogg, R.; Wilkins, R. G. Exchange Studies Of Certain Chelate Compounds Of The Transitional Metals. Part VIII. 2,2′,2″-Terpyridine Complexes. *J. Chem. Soc.* **1962**, 341–350.

23. Hoyler, R. H.; Hubbard, C. D.; Kettle, S. F. A.; Wilkins, R. G. The Kinetics of Replacement Reactions of Complexes of the Transition Metals with 2,2',2''-Terpyridine. *Inorg. Chem.* **1966**, *5* (4), 622–625.

24. Dobrawa, R.; Ballester, P.; Saha-Moeller, C. R.; Wuerthner, F. Thermodynamics of 2,2':6',2" - Terpyridine-Metal Ion Complexation, in Metal-Containing and Metallosupramolecular Polymers and Material; (Eds. U. S. Schubert, G. R. Newkome, I. Manners) *ACS Symposium Series 928;* American Chemical Society: Washington DC, 2006, Chapter 4, pp 43–62.

25. Dobrawa, R.; Wurthner, F. Metallosupramolecular Approach Toward Functional Coordination Polymers. *Polym. Sci., Part A: Polym. Chem.***2005**, *43* (21), 4981–4995.

26. Meier, M. A. R.; Lohmeijer, B. G. G.; Schubert, U. S. Relative Binding Strength of Terpyridine Model Complexes Under Matrix-Assisted Laser Desorption/Ionization Mass Spectrometry Conditions. *J. Mass Spectrom.* **2003**, *38* (5), 510–516.

27. Jackson, A. C.; Beyer, F. L; Price, S. C.; Rinderspacher, B. C.; Lambeth, R. H. Role of Metal–Ligand Bond Strength and Phase Separation on the Mechanical Properties of Metallopolymer Films. *Macromolecules* **2013**, *46*, 5416–5422.

28. Rowan, S. J.; Beck, J. B. Metal–Ligand Induced Supramolecular Polymerization: A Route To Responsive Materials. *Faraday Discuss.* **2005**, *128*, 43–53.

29. Ilavsky, J.; Jemian, P. R. J. Irena: Tool Suite for Modeling and Analysis of Small-Angle Scattering. *Appl. Crystallogr*. **2009**, *42*, 347−353.

30. Mugemana, C.; Guillet, P.; Hoeppener, S.; Schubert, U. S. Fustin, C.; Gohy, J. Metallo-Supramolecular Diblock Copolymers Based on Heteroleptic Cobalt(III) and Nickel(II) *Bis*-Terpyridine Complexes. *Chem. Commun.* **2010**, *46*, 1296–1298.

31. Brundle, C. R.; Chuang, T. J.; Wandelt, K. Core and Valence Level Photoemission Studies of Iron Oxide Surfaces and the Oxidation of Iron. *Surf. Sci.* **1977**, *68*, 459–468.

32. Volgman, K.; Voigts, F.; Maus-Friedrichs, W. The Interaction of H_2O Molecules With Iron Films Studied With MIES, UPS and XPS. *Surf. Sci.* **2012**, *606* (9), 858–864.

33. Umek, P.; Bittencourt, C.; Gloter, A.; Dominko, R.; Jagličić, Z.; Cevc, P.; Arcon, D. *J. Phys. Chem. C*. Local Coordination and Valence States of Cobalt in Sodium Titanate Nanoribbons. **2012**, *116*, 11357–11363.

34. Kochubey, D.; Kaichev, V.; Saraev, A.; Tomyn, S; Belov, A.; Voloshin, Y. Combined X-ray Absorption Near-Edge Structure and X-ray Photoelectron Study of the Electrocatalytically Active Cobalt(I) Cage Complexes and the Clathrochelate Cobalt(II)- and Cobalt(III)-Containing Precursors and Analogs. *J. Phys. Chem. C* **2013**, *117*, 2753–2759.

List of Symbols, Abbreviations, and Acronyms

AIBN	Azobisisobutyronitrile
DMA	dynamic mechanical analysis
DSC	differential scattering calorimetery
Hz	Hertz
MeBIP	2,6-bis(1’-methylbenzimidazolyl)pyridine
ML	metal-ligand
NMR	nuclear magnetic resonance
ppm	parts per million
PTHF	poly(tetrahydrofuran)
RAFT	reversible addition fragmentation chain transfer
SAXS	small-angle x-ray scattering
TPY	terpyridine
UV/Vis	ultraviolet/visible
WAXS	wide-angle x-ray scattering
XPS	x-ray photoelectron spectroscopy
XRD	x-ray diffraction

NO. OF COPIES	ORGANIZATION
1 (PDF)	DEFENSE TECHNICAL INFORMATION CTR DTIC OCA
1 (PDF)	DIRECTOR US ARMY RESEARCH LAB IMAL HRA
1 (PDF)	DIRECTOR US ARMY RESEARCH LAB RDRL CIO LL
1 (PDF)	GOVT PRINTG OFC A MALHOTRA
4 (PDF)	RDRL WMM G A JACKSON F BEYER RDRL WMM C V RODRIGUEZ SANTIAGO RDRL WMM F B G BUTLER

INTENTIONALLY LEFT BLANK.